Title:

Disrupted resting-state fMRI coherence at vasomotor frequency links carotid artery stenosis to functional connectivity loss

Authors:

Sangcheon Choi[1,2,8], Gabriel Hoffmann[1,2], Sebastian Schneider[1,2], Stephan Kaczmarz[1,2,3], Xin Yu[5], Christian Sorg[1,2,4,7], and Christine Preibisch[1,2,6,7]

Affiliations:

1 Institute for Neuroradiology, School of Medicine and Health, TUM University Hospital, Technical University of Munich, Munich 81675, Germany

2 TUM-Neuroimaging Center, School of Medicine and Health, Technical University of Munich, Munich 81675, Germany

3 Philips GmbH Market DACH, Hamburg 22335, Germany

4 Clinic for Psychiatry, School of Medicine and Health, TUM University Hospital, Technical University of Munich, Munich 81675, Germany

5 Athinoula A. Martinos Center for Biomedical Imaging, Department of Radiology, Harvard Medical School, Massachusetts General Hospital, Charlestown, MA 02129, USA

6 Clinic for Neurology, School of Medicine and Health, TUM University Hospital, Technical University of Munich, Munich 81675, Germany

7 These authors contributed equally to this work.

8 Lead Contact

***Lead corresponding author:**

Dr. Sangcheon Choi

Email: sc.choi@tum.de
Address: Ismaninger Str. 22, 81675 Munich, Germany

ABSTRACT

Vasomotor dynamics at the infra-slow frequencies (~0.1 Hz), driven by synchronized oscillation of smooth muscle cells in vessel walls, play an important role in regulating cerebral perfusion and constitute a physiological basis for resting-state functional connectivity (FC). Invasive animal studies have demonstrated that vasomotor activity contributes to coherent blood oxygenation-dependent level (BOLD) signal fluctuations. However, in humans, it remains challenging to non-invasively detect this contribution due to the limited spatiotemporal sensitivity of functional magnetic resonance imaging (fMRI) to vasomotion. Leveraging internal carotid artery stenosis (ICAS) as a natural lesion model of impaired vasomotion, we examined whether impaired vasomotor activity influences inter-hemispheric BOLD coherence at ~0.1 Hz. Using a multi-modal fMRI framework that integrates resting-state fMRI with quantitative multi-parametric mapping of cerebral blood volume, blood flow, oxygen metabolism, and BOLD time lag, we compared BOLD coherence in patients with unliteral ICAS to healthy controls. Frequency-specific coherence analysis revealed significantly diminished inter-hemispheric BOLD coherence at the vasomotor frequency range (~0.1 Hz) across canonical resting-state networks in ICAS patients, whereas ultra-slow (<0.05 Hz) coherence remains largely preserved. This reduction was spatially widespread and particularly pronounced inside watershed areas, i.e., border zones between major vascular perfusion territories that are especially vulnerable to hypoperfusion and associated with a significantly increased lateralization in cerebral blood volume ($p < 0.01$) inside watershed areas. Notably, coherence-based FC patterns at ~0.1 Hz were heterogeneous inside watershed areas and homogeneous outside watershed areas, suggesting an interplay between compensatory mechanisms and vasomotion impairment. Taken together, our findings demonstrate that frequency-resolved, region-specific analysis can capture presumably vasomotion-related oscillatory signals at ~0.1 Hz and detect subtle differences in inter-hemispheric FC, offering a non-invasive biomarker for early cerebrovascular dysfunction, particularly in patients with ICAS and other vasomotion-related neuropathologies.

Keywords: resting-state fMRI, vasomotion, inter-hemispheric coherence, internal carotid artery stenosis (ICAS), watershed areas.

INTRODUCTION

Vasomotor activity arises from synchronized oscillations of smooth muscle cells in vascular walls and plays a fundamental role in regulating cerebral blood flow (CBF) (Nicoll and Webb 1955; Intaglietta 1990; Aalkjær, Boedtkjer, and Matchkov 2011). These oscillatory vasomotor signals reflect underlying vascular conditions and have been widely observed across species, including humans (Nicoll and Webb 1955; Rosenblum, Bonner, and Oldfield 1987; Seifert, Jager, and Bollinger 1988; Intaglietta 1990; Hudetz, Roman, and Harder 1992; Mayhew et al. 1996; Mitra et al. 1997; Kleinfeld et al. 1998; Obrig et al. 2000b; Razavi et al. 2008; Rayshubskiy et al. 2014; Broggini et al. 2024). In animals, invasive techniques such as laser Doppler flowmeter and optical recording have demonstrated that cerebral vasomotor activity typically exhibits slow oscillations peaking around 0.1 Hz within the infra-slow frequency band (Hudetz, Roman, and Harder 1992; Mayhew et al. 1996; Kleinfeld et al. 1998; Mateo et al. 2017; Broggini et al. 2024). Importantly, beyond its established role in regulating local cerebral perfusion, vasomotor activity has also been proposed as a physiological basis for functional connectivity (FC) during resting-state (Mateo et al. 2017). This hypothesis is primarily supported by evidence that spontaneous vasomotor oscillations, synchronized across homotopic cortical regions (i.e., symmetric regions in both hemispheres) and induced by ongoing neuronal activity, contribute to coherent blood oxygenation dependent level (BOLD) functional magnetic resonance imaging (fMRI) signals underlying resting-state functional connectivity (FC) in awake rodents as demonstrated in invasive optical imaging (Mateo et al. 2017; Drew et al. 2020; Broggini et al. 2024). Coherence-based analysis has further demonstrated that spontaneous arteriole diameter oscillations, driven by vasomotion in the infra-slow frequency range (~0.1 Hz), can modulate BOLD fMRI signal coherence, particularly in homotopic cortical regions (Mateo et al. 2017; Drew et al. 2020). Notably, a distinct peak in power spectral density (PSD) near 0.1 Hz has been observed in the somatosensory cortex of anesthetized rats, suggesting that inter-hemispheric FC can be strengthened through vasomotion-related mechanisms (Williams et al. 2010; Choi et al. 2023).

However, in humans, the contributions of vasomotion to resting-state BOLD FC remain largely speculative, primarily due to technical challenges in measuring vasomotion non-invasively. Under intraoperative conditions, a few invasive human studies have reported spatially distinct vasomotor oscillations across the cortex at the vasomotor frequency (~0.1 Hz) (Rosenblum, Bonner, and Oldfield 1987; Rayshubskiy et al. 2014). Despite these observations, evidence linking vasomotor activity to resting-state BOLD FC in humans using non-invasive fMRI remains scarce (Mitra et al. 1997; Razavi et al. 2008; Rayshubskiy et al. 2014). Vasomotor activity, which regulates the arterial reservoir volume (Nicoll and Webb 1955) and is considered ubiquitous in vascular structures (Broggini et al. 2024) and may serve as a potential biomarker of cerebrovascular dysfunction. Indeed, disrupted vasomotor activity has been observed in both high-risk stroke mouse models (Zhang et al. 2024) and in patients with internal carotid artery stenosis (ICAS) (Silvestrini et al. 1996; Gur, Bova, and Bornstein 1996; Silvestrini et al. 2000; Gur and Bornstein 2006; Avirame et al. 2015). Given the evidence of vasomotor impairment in patients with ICAS, it is plausible that inter-hemispheric resting-state (rs-) fMRI coherence, particularly in the ~0.1 Hz frequency band, may be altered in patients with ICAS and could serve as a frequency-specific signature of cerebrovascular dysfunction. Therefore, the present study leverages ICAS as a natural lesion model of vasomotor dysfunction.

Moreover, multi-parametric hemodynamic MRI studies have revealed unilateral vascular-hemodynamic impairments in CBF and cerebral blood volume (CBV) in patients with asymptomatic unilateral ICAS (Gleissner et al. 2022; Kaczmarz et al. 2021; Kaczmarz et al. 2018; Gottler et al. 2019; Schneider et al. 2022; Schneider et al. 2023), while the cerebral metabolic rate of oxygen ($CMRO_2$) remains largely preserved, suggesting intact neuronal function (Gottler et al. 2020). The most pronounced alterations in CBF and CBV have been observed in watershed areas, i.e., cortical and internal border zones between major perfusion territories that are particularly vulnerable to hypoperfusion (Kaczmarz et al. 2021), suggesting that vasomotor activity may be reflected in macroscopic CBV measures (He et al. 2018; Holstein-Ronsbo et al. 2023; Kilic and Devor 2023). In addition, disrupted coupling between CBF and $CMRO_2$ has been reported in the ICAS patients, indicating altered flow-metabolism dynamics (Gottler et al. 2019). Although correlation-based rs-fMRI analyses have shown that vasomotor impairment is strongly associated with decreased FC in patients with high-grade ICAS (Avirame et al. 2015), minimal or no group-level differences in homotopic correlation between healthy controls and ICAS patients (after controlling for hemodynamic impairments) suggest that vascular-hemodynamic impairments may influence resting-state FC in more subtle or complex ways (Schneider et al. 2022; Schneider et al. 2023).

Taken together, these findings suggest that inter-hemispheric coherence of rs-fMRI signals in patients with asymptomatic unilateral ICAS may be altered in both frequency-specific and spatially dependent ways. We therefore hypothesize that vasomotor impairments in these patients lead to spectrally and spatially specific alterations in inter-hemispheric resting-state BOLD FC. Furthermore, we propose that frequency-resolved coherence analysis can uncover subtle but meaningful disruptions in brain networks that may not be detectable using conventional correlation methods, providing new insights into the physiological basis of FC in the human brain. As illustrated in **Fig. 1**, our investigation is guided by three central hypotheses regarding the impact of unilateral ICAS: 1) Frequency specificity: We hypothesize that the most prominent alterations in BOLD signal oscillations and coherence will occur in the ~0.1 Hz frequency range, which has been associated with vasomotion (Avirame et al. 2015; Mateo et al. 2017), whereas ultra-slow coherence below 0.05 Hz, reflecting neuronal activity (He et al. 2018) and arousal brain state (Raut et al. 2021) will remain largely preserved. 2) Brain-wide effect: We hypothesize that vasomotion-related disruptions in inter-hemispheric coherence will be spatially widespread across the whole brain (Mitra et al. 1997; Razavi et al. 2008; Broggini et al. 2024). 3) Regional vulnerability: We hypothesize that BOLD signal fluctuations, inter-hemispheric coherence alterations, and corresponding changes in vasomotion-related hemodynamic parameters, particularly CBV, will be concentrated in vulnerable vascular territories such as watershed areas, which have been previously demonstrated to be most affected by hypoperfusion (Torvik 1984; Bilecen et al. 2002; Kaczmarz et al. 2021).

In this study, we combined rs-fMRI with quantitative hemodynamic MRI to investigate how asymptomatic unilateral ICAS alters frequency-specific inter-hemispheric BOLD signal coherence and its coupling to cerebral perfusion parameters. To test our hypotheses (**Fig. 1**), we developed a novel analytic framework integrating rs-fMRI-based spectral power spectral density (PSD) and coherence analysis with multi-parametric MRI maps including relative CBV, CBF, relative $CMRO_2$, and BOLD time lag (i.e., relative time lag of cortical regions to the sagittal superior sinus) in both healthy controls and patients with unilateral ICAS, particularly inside watershed areas as well as across resting-state brain networks. To assess frequency specificity (hypothesis 1), we compared inter-hemispheric PSD and coherence between healthy controls and patients with asymptomatic unilateral ICAS across distinct frequency bands (<0.05 Hz and ~0.1 Hz) and across both homotopic and heterotopic regions of interest (ROI) pairs. To assess brain-wide

effects (hypothesis 2), we analyzed inter-hemispheric coherence patterns across intrinsic resting state networks defined by Yeo and colleagues (Yeo et al. 2011). Finally, to assess regional vulnerability (hypothesis 3), we compared inter-hemispheric PSD, coherence, and quantitative hemodynamic parameters between regions of distinct perfusion (Seifert, Jager, and Bollinger 1988), specifically inside versus outside watershed areas, i.e., vascular border zones that are particularly vulnerable to reductions in CBF in patients with ICAS (Kaczmarz et al. 2021). Our findings not only offer new insights into the impact of vascular impairment on frequency-resolved brain network dynamics and distinct perfusion territories but also highlight the potential of inter-hemispheric coherence at vasomotor frequencies as a distinct, non-invasive biomarker for early cerebrovascular dysfunction.

RESULTS

Frequency-specific disruption of inter-hemispheric BOLD coherence at vasomotor frequency (~0.1 Hz) in patients with unilateral ICAS

We developed a multi-modal fMRI approach to assess whole-brain BOLD rs-fMRI signals and multi-parametric quantitative hemodynamic MRI maps to test our hypotheses (**Fig. 1**) in healthy controls and patients with asymptomatic unilateral ICAS (**Fig. 2A**). For inter-hemispheric ROI-based analysis, we employed an Atlas of Intrinsic Connectivity of Homotopic Areas (AICHA) (Joliot et al. 2015), extracting fMRI time series from individual AICHA-defined ROIs (**Fig. 2B-C**). To test our first hypothesis that inter-hemispheric rs-fMRI coherence may be impaired in the vasomotor frequency band around ~0.1 Hz (Mateo et al. 2017), we compared power spectral densities (PSDs) across the two hemispheres, as well as inter-hemispheric coherence, between healthy controls and patients with unilateral ICAS across the infra-slow oscillatory frequency band (<0.1 Hz). Using the AICHA atlas (Joliot et al. 2015) (**Fig. 2B**), we first analyzed the temporal oscillatory patterns and frequency responses of rs-fMRI signals between the right (in patients, ipsilateral to the stenosis) and left hemispheres. In representative subjects from each group, we computed the ROI-average, Z-score normalized rs-fMRI time series for both hemispheres and compared the correlation and coherence values between them. As illustrated in **Fig. 2D-E**, the patient with ICAS exhibited weaker synchronization and less pronounced oscillatory patterns, resulting in lower correlation and coherence values, compared to the healthy control. To further examine frequency-specific effects, we computed PSDs separately for the right and left hemispheres. In both subjects, robust PSD peaks were observed at 0.01-0.05 Hz (referred to as <0.5 Hz) (**Fig. 2F**). However, a distinct alteration of PSD in the 0.08-0.1 Hz range (referred to as ~0.1 Hz) was noted in the ICAS patient, potentially reflecting dampened vasomotor activity (details in the Discussion). For group-level analysis, we calculated the absolute inter-hemispheric differences in PSDs ($|\Sigma(\Delta_{LR}\ \mathrm{PSD})|$) for both frequency bands (<0.5 Hz and ~0.1 Hz). Notably, a significant group difference emerged in the vasomotor frequency band, ~0.1 Hz, with ICAS patients showing significantly stronger inter-hemispheric asymmetry compared to healthy controls (**Fig. 2G**), supporting a frequency-specific disruption of functional coherence in ICAS.

To investigate alterations in inter-hemispheric FC in patients with ICAS, we analyzed Z-score normalized rs-fMRI time series for homotopic and heterotopic AICHA ROI pairs in the representative subjects shown in **Fig. 2E**. Based on correlation coefficients from the representative healthy control, we selected two AICHA ROI pairs, i.e., #1: Precuneus, #2: Lingual (**Fig. 2H-I**), which showed the highest homotopic correlation. We first examined homotopic rs-fMRI time series from the Precuneus ROI pair and compared correlation and coherence values between the two signals. As shown in **Fig. 2J**, the ICAS patient (right)

exhibited synchronized but visibly weaker oscillatory temporal patterns compared to the healthy control (left). While the correlation coefficients were identical (control: 0.95; patient: 0.95), the coherence was notably reduced in the patient (control: 0.93; patient: 0.88), suggesting frequency-specific decoupling between the two hemispheres. Next, we assessed heterotopic rs-fMRI time series from the Precuneus and Lingual ROIs. As illustrated in **Fig. 2K**, the ICAS patient (right) showed markedly reduced synchronized and oscillatory temporal patterns, with both correlation and coherence values lower than those observed in the healthy control (left; correlation: control 0.72 vs. patient 0.53, coherence: control 0.51 vs. patient 0.40). These findings suggest that ICAS may differentially influence inter-hemispheric FC relying on the spatial relationship and spectral dynamics of the ROI pair.

We further conducted a group-level analysis of inter-hemispheric coherence across the infra-slow oscillatory frequency range (0.01-0.1 Hz, referred to as <0.1 Hz) in healthy controls and patients with unilateral ICAS. To compare coherence between the two groups, Fisher Z-transformed coherence coefficients were computed between homotopic ROI pairs. As shown in **Fig. 2L**, group-averaged spectral coherence analysis revealed prominently reduced coherence values in the ICAS group, specifically in the 0.08-0.1 Hz range (~0.1 Hz), while both groups exhibited similar coherence patterns in the ultra-slow frequency band (0.01-0.05 Hz). Statistical analyses confirmed that homotopic coherence was significantly lower in patients with ICAS than in healthy controls in the 0.08-0.1 Hz band (highlighted by a blue box in **Fig. 2M**). Similarly, heterotopic coherence analysis also showed a significant group difference at 0.08-0.1 Hz (**Fig. 2N**).

In summary, supporting our first hypothesis, these findings indicate that the disruption of inter-hemispheric coherence in patients with ICAS is frequency-specific, centered around ~0.1 Hz, corresponding to the known range of vasomotor activity (Mateo et al. 2017). Moreover, the results clearly differentiate spectral coherence FC at ~0.1 Hz between patients with ICAS and healthy controls.

Brain-wide mapping of inter-hemispheric coherence across canonical rs-fMRI networks at ultra-slow (<0.05 Hz) and vasomotor (~0.1 Hz) frequency bands

Based on the inter-hemispheric PSD and coherence analysis, we examined the frequency-dependent coherence across large-scale networks in healthy controls and patients with unilateral ICAS. To define inter-hemispheric rs-fMRI networks, we employed seven canonical rs-fMRI networks proposed by Yeo and colleagues (Yeo et al. 2011). The seven rs-fMRI networks consisted of: Default Mode Network (DMN), Somatomotor Network (SMN), Dorsal Attention Network (DAN), Visual Network (VIN), Salience Network (SAN), Limbic Network (LIN), and Executive Control Network (ECN). In addition, the subcortical network (SubCort) was included in the analysis. Each AICHA ROI was assigned to one of these canonical rs-fMRI networks following the procedures described by Labache et al. (Labache et al. 2023) (**Fig. 3A** and **Table S1**). For network-level analysis of homotopic and heterotopic FC, we first visualized coherence matrices across the Yeo-defined networks for both groups at full infra-slow oscillatory frequency band (0.01-0.1 Hz). Interestingly, lower coherence values were observed in the ICAS group for heterotopic ROI pairs, particularly across VIN, SMN, and DAN (**Fig. 3B**). To examine frequency-specific patterns, we re-calculated inter-hemispheric coherence matrices at two distinct frequency bands: <0.05 Hz and ~0.1 Hz. This analysis revealed notably diminished homotopic and heterotopic coherence across all networks in the ICAS group at vasomotor frequency band (~0.1 Hz), while coherence pattens at ultra-slow frequency band (<0.05 Hz) remained largely comparable between the two groups (**Fig. 3C** and **E**).

To reduce noise and thus more clearly compare the coherence patterns across networks between the two groups, the ROI-based inter-hemispheric coherence matrices were averaged within each of the predefined networks (**Fig. 3D** and **3F**). At <0.05 Hz, both groups exhibited similar inter-hemispheric coherence patterns, with strong coherence observed along homotopic network pairs (diagonal) and across heterotopic connections involving the VIN, SMN, DAN, and SAN (upper four networks in the off-diagonal) (**Fig. 3D** and **S1 A**). No significant differences in inter-hemispheric coherence were observed between the two groups in this frequency band (**Fig. 3G**). In contrast, at ~0.1 Hz, distinct coherence patterns emerged between the two groups and the ICAS group displayed globally reduced inter-hemispheric coherence, both in homotopic (diagonal) and heterotopic (off-diagonal) networks (**Fig. 3F and S1 B**). Statistically, significant reductions in coherence were found in the VIN, SMN, DAN, and ECN in patients with ICAS (**Fig. 3H**).

In summary, supporting our second hypothesis regarding spatially organized functional networks, these results demonstrate that frequency-specific disruptions in inter-hemispheric coherence at ~0.1 Hz (i.e., vasomotor frequency band) are consistently observed across the large-scale intrinsic brain networks. Moreover, the network-level coherence alterations at ~0.1 Hz can clearly be distinguished from those at <0.05 Hz (ultra-slow frequency band), highlighting the functional significance of frequency-dependent FC alteration in patients with ICAS.

Regional vulnerability of inter-hemispheric BOLD coherence and vascular impairment inside watershed areas in patients with ICAS

To further explore regional effects on inter-hemispheric coherence, we investigated the impact of distinct perfusion conditions, i.e., inside vs. outside watershed areas, on frequency-dependent inter-hemispheric coherence in both healthy controls and patients with unilateral ICAS. As illustrated in **Fig. 4A**, we identified ROIs overlapping with pre-defined watershed areas using the AICHA atlas (Joliot et al. 2015) (n = 41 ROIs, details in the **Methods**). These ROIs were used to assess frequency-dependent inter-hemispheric coherence and to evaluate regional quantitative hemodynamic MRI parameters such CBV, CBF, $CMRO_2$ and BOLD time lag (**Fig. 4A**). As shown in **Fig. 4B**, we quantified the distribution of the canonical rs-fMRI networks within the watershed areas: VIN: 54.3%, SMN: 4.8%, DAN: 15.8%, SAN: 0.0%, LIN: 22.2%, ECN: 38.9%, DMN: 10.0%, and SubCort: 13.6%. Notably, no ROI from SAN overlapped with the watershed area (**Table S2**).

To characterize spectral dynamics inside and outside watershed areas (**Table S2-3**), we computed group-averaged inter-hemispheric PSD differences ($|\Sigma(\Delta_{LR}\ PSD)|$) at the two distinct frequency bands (ultra-slow; <0.5 Hz and vasomotor; ~0.1 Hz) for healthy controls and patients with ICAS. Notably, inside watershed areas, a significant group difference was observed only at ~0.1 Hz, whereas no significant differences were found at <0.05 Hz inside the watershed area, nor at either frequency band outside the watershed area (**Fig. 4C**). We also assessed group-averaged inter-hemispheric coherence in the same two frequency bands, again separately for regions inside and outside watershed areas. Consistent with the PSD results, significant group differences in both homotopic and heterotopic coherences were observed only at ~0.1 Hz inside the watershed area. In contrast, coherence values at ~0.1 Hz outside watershed areas, as well as at <0.05 Hz both inside and outside the watershed areas, did not differ significantly between the two groups (**Fig. 4D**, **S2**, and **S3**).

To further examine regional differences in inter-hemispheric coherence, we mapped coherence matrices across the canonical rs-fMRI networks separately for regions inside and outside watershed areas. For the

two groups, network-averaged coherence matrices were computed at the two distinct frequency bands (<0.05 Hz and ~0.1 Hz). As shown in **Fig. 4E**, inside the watershed areas, overall coherence values at ~0.1 Hz were markedly diminished and spatially heterogeneous across the networks (with the exception of the SAN, which contained no ROI). The SubCort network exhibited low homotopic (diagonal) and heterotopic (off-diagonal) coherence values. These reductions are also visualized in the circular diagram, which illustrates pronounced decreases in inter-hemispheric coherence inside the watershed areas. Statistically, significantly lower coherence coefficients were observed in patients with ICAS across the seven cortical networks (except DAN and SAN; SAN was not assigned) at ~0.1 Hz (**Fig. 4G**), underscoring the impact of regional perfusion impairment on frequency-specific inter-hemispheric FC. In contrast, outside the watershed areas (**Fig. 4F**), coherence values at ~0.1 Hz were only moderately reduced and were more homogeneous across heterotopic connections, while homotopic coherence remained relatively strong across most networks. The corresponding circular diagram confirms a lower degree of coherence reduction outside watershed areas compared to inside watershed areas. Only two networks, i.e., SMN and DAN, showed significantly lower inter-hemispheric coherence in patients with ICAS outside the watershed area (**Fig. 4H**).

In addition, to investigate the impact of distinct perfusion territories (i.e., inside vs. outside watershed areas) on multi-parametric quantitative hemodynamic MRI parameters, we first estimated relative CBV, CBF, relative $CMRO_2$, and BOLD time lag maps in healthy controls and patients with unilateral ICAS (**Fig. S4**). For each parameter, absolute inter-hemispheric differences were calculated by summing the difference between left and right hemispheres across homotopic ROI pairs: $|\Sigma(\Delta_{LR}\ CBV)|$, $|\Sigma(\Delta_{LR}\ CBF)|$, $|\Sigma(\Delta_{LR}\ CMRO_2)|$, and $|\Sigma(\Delta_{LR}\ \text{BOLD lag})|$ (details in **Methods**). These metrics were then compared between the two groups, separately for inside and outside of watershed areas (**Fig. 4I-J**). Interestingly, the inter-hemispheric difference in relative CBV, $|\Sigma(\Delta_{LR}\ CBV)|$ showed a prominent and statistically significant group difference inside the watershed areas ($p < 0.01$), but not outside. In contrast, CBF differences were significant in both regions ($p < 0.05$), showing diminished perfusion in the hemisphere ipsilateral to the stenosis (**Fig. S4 B**), while relative $CMRO_2$ differences did not reach statistical significance in either region. This finding may indicate a generalized disruption of flow-metabolism coupling in patients, regardless of perfusion territory, consistent with previous findings (Gottler et al. 2019). For BOLD time lag, a significant inter-hemispheric difference was observed only outside the watershed areas ($p < 0.05$), while no significant difference was found inside the watershed areas, possibly reflecting asymmetric blood arrival times: the hemisphere ipsilateral to the stenosis show delayed perfusion outside the watershed territory, whereas both hemispheres exhibited more symmetric prolonged arrival times within the watershed areas (**Fig. S4 D**).

Taken together, in support of our third hypothesis regarding regions of distinct perfusion alterations, these findings demonstrate that aberrant inter-hemispheric rs-fMRI coherence at vasomotor frequency band (~0.1 Hz) is localized specifically to vulnerable regions at the border of vascular territories, i.e., the watershed areas, that are particularly affected by hypoperfusion. Importantly, this ~0.1 Hz-specific disruption in coherence appears to be independent of canonical rs-fMRI network organization. Furthermore, the results highlight the vulnerability of the watershed areas (Kaczmarz et al. 2021) in patients with unilateral ICAS, which are closely associated with a lateralized increase in CBV.

DISCUSSION

Guided by our three hypotheses, i.e., frequency specificity, brain-wide effect, and regional vulnerability, this study demonstrates that frequency-specific alterations in inter-hemispheric PSD and coherence at the

vasomotor frequency band (~0.1 Hz) distinguish patients with unilateral ICAS from healthy controls, despite preserved coherence at the ultra-slow frequency band (<0.05 Hz). Using our integrated multi-modal rs-fMRI method, we demonstrate that inter-hemispheric coherence at ~0.1 Hz is disrupted across canonical intrinsic networks and exhibits pronounced reduction in watershed areas, i.e., regions with particular perfusion vulnerability (Kaczmarz et al. 2021), where inter-hemispheric coherence is prominently diminished and CBV lateralization significant. These findings not only bridge a gap in understanding how ICAS impacts brain-wide vasomotion-related coherence, particularly in perfusion-vulnerable territories (watershed areas), but also highlight the potential of rs-fMRI coherence at ~0.1 Hz as a non-invasive biomarker for early cerebrovascular dysfunction.

Our multi-modal fMRI analysis reveals notably desynchronized time series, diminished coherence matrices, and lateralized PSDs at ~0.1 Hz in patients with unilateral ICAS, accompanied by impaired CBV inside watershed areas. While these findings provide indirect evidence for vasomotor dysfunction, interpretation of the physiological basis of ~0.1 Hz oscillations require caution. Vasomotor activity plays a key role in regulating arterial reservoir volumes and maintaining the homeostasis of flow and pressure in vascular networks (Nicoll and Webb 1955; Intaglietta 1990). However, since BOLD fMRI signals predominantly reflect venous rather than arterial dynamics (He et al. 2018), interpreting vasomotion influences on BOLD coherence requires an appreciation of vessel-specific contributions. While arteries with smooth muscle cells generate vasomotor activity, capillaries (without muscle cells) lack such capability and only show passive responses due to homeostasis. Importantly, venules and veins also have smooth muscle cells (Boittin et al. 1999) and can regulate vasomotor activity, supporting venous return (Nicoll and Webb 1955; Aalkjær, Boedtkjer, and Matchkov 2011). In addition, prior studies have supported the existence of venous vasomotor activity (Jones 1852; Wiedeman 1957; Gotoh et al. 1982; Hundley et al. 1988). Thus, as proposed by Mateo et al (Mateo et al. 2017), impaired vasomotor oscillations may manifest in the BOLD fMRI signals as reduced inter-hemispheric coherence at ~0.1 Hz. Our findings further support this hypothesis by linking vasomotor impairments in ICAS patients to both ~0.1 Hz-specific PSD and CBV asymmetries, particularly inside watershed areas. In this study, we define the ~0.1 Hz band as the 0.08-0.1 Hz, situated within the typical resting-state fMRI frequency band (0.01-0.1 Hz) (Fox and Raichle 2007), to specifically probe vasomotor-related fluctuations. Notably, spectral peaks of vasomotor activity in the 0.08-0.1 Hz range have been consistently observed in previous studies employing fMRI (Mitra et al. 1997), near infrared spectroscopy (Obrig et al. 2000a), and multi-spectral optical intrinsic signal imaging (Rayshubskiy et al. 2014) in humans.

In contrast to this clear FC disruption at ~0.1 Hz, ultra-slow oscillations (<0.05 Hz) remained stable in patients with ICAS (**Fig. 2L**, **3C-D**, and **3G**). This stable ultra-slow oscillations, together with preserved $CMRO_2$ (**Fig. 4I-J**), suggest preserved neuronal activity (He et al. 2018) and global arousal brain state via neuromodulators, such as adrenergic and cholinergic neurons (Raut et al. 2021; Reimer et al. 2016). This pattern followed a spatial gradient from strong to weak coherence, spanning from unimodal (VIN and SMN), multi-modal (DAN and SAN), to transmodal (ECN and DMN) networks, reflecting know functional hierarchies and principal gradient axes (Raut et al. 2021; Margulies et al. 2016). Moreover, the preserved ultra-slow oscillations align with previous laminar fMRI findings (Choi et al. 2022; Choi et al. 2023). Further, differences in ultra-slow coherence between cortical and subcortical structures may reflect distinct neurovascular coupling mechanisms (**Fig. 3D**). Altogether, these results highlight not only neuronal resilience at ultra-slow frequency band but also vascular vulnerability at vasomotor frequency range, particularly inside watershed areas.

Watershed regions are of particular clinical relevance in ICAS patients (Torvik 1984; Kaczmarz et al. 2018; Kaczmarz et al. 2021). Inside watershed areas, coherence matrices at ~0.1 Hz showed pronounced spatial heterogeneity across networks, consistent with the more severe hemodynamic impairments reported in prior work (Kaczmarz et al. 2018; Kaczmarz et al. 2021) (**Fig. 4E**). This heterogeneity likely reflects an interplay between compensation mechanisms (e.g., collateralization and autoregulation) (Zarrinkoob et al. 2019; Reinhard et al. 2003) and impaired vasomotor control (Nicoll and Webb 1955; Intaglietta 1990; Aalkjær, Boedtkjer, and Matchkov 2011). In contrast, coherence at ~0.1 Hz outside watershed areas was spatially homogeneous and relatively preserved (**Fig. 4F**), although diminished coherence at ~0.1 Hz was observed in SMN and DAN outside watershed areas, potentially due to age-related limitations in compensatory capacity in ICAS patients (**Fig. 4H**). These observations suggest that ~0.1 Hz-related coherence could serve as a sensitive marker of regional vulnerability to vascular impairment in ICAS patients, highlighting the increased sensitivity inside watershed areas.

A major methodological strength of this study is the integration of frequency-specific rs-fMRI analysis with multi-parametric hemodynamic MRI, enabling the identification of vasomotion-related disruptions in functional dynamics and region-specific vascular vulnerabilities, particularly inside watershed areas. By examining PSD and coherence at two distinct frequency bands, i.e., ultra-slow (<0.05 Hz) and vasomotor (~0.1 Hz), and linking these metrics to quantitative maps of CBV, CBF, $CMRO_2$, and BOLD time lag, we demonstrated that inter-hemispheric desynchronization at ~0.1 Hz is specifically associated with ipsilaterally increased CBV, as a potential factor related to impaired vasomotion due to chronic vasodilation. In contrast, conventional correlation-based FC measures failed to detect significant group differences between healthy controls and ICAS patients (Schneider et al. 2022; Schneider et al. 2023) (**Fig. S5**), due to their limited sensitivity to frequency-specific impacts on FC. Our multi-modal fMRI framework, therefore, extends beyond conventional correlation-based approaches, enabling the investigation of brain-wide, frequency-specific functional dynamics and vascular contributions to rs-fMRI signals in ICAS patients. In the future, coherence-based fMRI may offer valuable insights for detecting subtle vascular impairment and functional desynchronization in patients with neurological and neurovascular disorders, including but not limited to ICAS.

While this study clearly identified frequency-specific coherence disruption at ~0.1 Hz, it remains an indirect measure of vasomotor activity. Several potential confounds may influence signal fluctuations within this frequency range. First, cardiac pulsation (~1 Hz) could introduce aliasing artifacts, particularly given the Nyquist sampling limit of rs-fMRI signals (~0.4 Hz) (Chang, Cunningham, and Glover 2009; Birn 2012; Caballero-Gaudes and Reynolds 2017). Second, Mayer waves (i.e., spontaneous oscillations in arterial blood pressure) may overlap at the same frequency range (~0.1 Hz) (Julien 2006). Third, the bandpass filtering during preprocessing (0.01-0.1 Hz) may modulate the spectral profile at the upper boundary of the frequency range. However, these confounding factors are unlikely to account for the observed group difference or spatial specificity in vascularly vulnerable territories (i.e., watershed areas), as such artifacts would be expected to affect both patient and control groups equally. Moreover, while coherence analysis reveals disrupted FC in ICAS patients, it cannot fully disentangle causality between impaired vasomotor activity and disrupted coherence at ~0.1 Hz. Future work should explore the causality by comparing vasomotor activity between pre- and post-revascularization in ICAS patients (Cheng et al. 2012) or by incorporating concurrent transcranial Doppler measurements to directly assess vasomotor activity alongside our multi-modal fMRI framework. Additionally, animal models with experimentally induced ICAS (Ishikawa et al. 2023) (see **Fig. S6**) could also provide direct evidence for the relationship between

vasomotion impairments and inter-hemispheric coherence disruption when combined with concurrent optical recording.

In conclusion, our study demonstrates that inter-hemispheric BOLD coherence at ~0.1 Hz may serve as a frequency-sensitive and spatially specific marker of cerebrovascular dysfunction in patients with unilateral ICAS. These findings help bridge the gap between vascular pathology and resting-state functional disruption, and highlight the potential of coherence-based spectral analysis as a non-invasive biomarker not only for ICAS but also for other clinical conditions associated with vasomotion impairments, including stroke, small vessel disease, dementia, and Alzheimer's Disease (Zhang et al. 2024; Wardlaw, Smith, and Dichgans 2019; Holstein-Ronsbo et al. 2023; Di Marco et al. 2015).

MATERIALS and METHODS

In this study, we analyzed a subsample of existing multi-modal MRI data from our previous study, from which different aspects have already been published (Gottler et al. 2020; Gleissner et al. 2022; Kaczmarz et al. 2021; Kaczmarz et al. 2018; Gottler et al. 2019; Schneider et al. 2022; Schneider et al. 2023).

SUBJECT DETAILS AND MULTI-MODAL MRI DATA ACQUISITION

Subjects

All participants provided written informed consent prior to scanning in accordance with the policies of the institution's Human Research Committee. The study was approved by the Institutional Review Board of the Klinikum rechts der Isar at Technical University of Munich. Patients with unilateral asymptomatic ICAS were recruited through the outpatient clinic for carotid stenoses at the Department of Vascular and Endovascular Surgery, while healthy control participants were recruited via word-of-mouth advertisement. As previously reported (Gottler et al. 2020; Gleissner et al. 2022; Kaczmarz et al. 2021; Kaczmarz et al. 2018; Gottler et al. 2019; Schneider et al. 2022; Schneider et al. 2023), the study enrolled 29 patients with high-grade, unilateral, asymptomatic ICAS (confirmed by duplex ultrasonography; all >70% stenosis based on NASCET criteria (NASCET 1991)) and 30 age-matched healthy controls. Each participant underwent a clinical assessment that included a medical history review, basic neurological and psychiatric screening, and an MRI scan. Patients were classified as clinically asymptomatic if they exhibited no neurological symptoms such as stroke, transient ischemic attack (TIA), or paresis. Individuals with a history of neurological or psychiatric disorders, clinically significant structural brain abnormalities, or MRI contraindications were excluded. Due to insufficient MRI data quality, two patients and four healthy controls were excluded from the analysis, resulting in a final sample of 27 patients (11 females; mean age 70.3 ± 7.2 years) and 26 healthy controls (15 females; mean age 70.3 ± 4.8 years). Detailed demographic information was described in Supplementary Information (**Table S4**).

Multi-modal rs-fMRI and multiparametric quantitative MRI data acquisition

All MRI data were acquired on a whole-body 3T Ingenia MRI scanner (Philips Healthcare, Best, The Netherlands) equipped with a 16-channel (dynamic susceptibility contrast (DSC) MRI) or a 32-channel head coil (for others) (**Fig. 2A**). Detailed acquisition parameters are described in the Supplementary Information. In short: For assessing power spectral density (PSD), coherence of BOLD fMRI signal time series, T2*-weighted multiband echo planar imaging (EPI) data were acquired under resting-state conditions. The acquisition parameters were as follows: repetition time (TR) = 1200 ms, echo time (TE) =

30 ms, total acquisition time = 10 minutes, flip angle (FA) = 70°, multiband factor = 2, SENSE factor = 2, 38 slices, matrix size = 192x192, voxel size = 3x3x3 mm^3, and 500 dynamic scans. For the anatomical reference (**Fig. 2B**), T1-weighted magnetization prepared rapid gradient echo (MPRAGE) data were acquired with 170 sagittal slices (**Fig. 2C**).

Quantitative perfusion and oxygenation parameter were acquired and processed as described in detail previously (Gottler et al. 2019; Kaczmarz et al. 2021; Schneider et al. 2023). Relative CBV was derived from DSC MRI data following bolus injection of gadolinium-based contrast agent (Gd-Dota; concentration 0.5 mmol/ml, dose 0.1 mmol/kg, minimum 7.5 mmol per subject). CBF was measured using pseudo-continuous arterial spin labeling (pCASL) sequence in accordance with the ISMRM Perfusion Study Group consensus recommendations (Alsop et al. 2015) using a prolonged post-labeling delay of 2000 ms and applying background suppression. The oxygen extraction fraction (OEF) was calculated from R2′ ($= 1/T2^* - 1/T2$) and CBV, where $T2^*$ and $T2$ were derived from separate GRE and GRASE sequences, respectively, according to the multiparametric quantitative BOLD approach (Kaczmarz, Hyder, and Preibisch 2020). Relative $CMRO_2$ was then estimated from the product of relative OEF and CBF (Rodgers, Detre, and Wehrli 2016; Biondetti, Cho, and Lee 2023).

DATA PROCESSING

All data processing was performed using MATLAB (Mathworks, Natick, MA, version R2023a), Python (version 3.9.13), and R (version 4.4.0). Detailed descriptions of the processing and analysis workflows have been published in previous studies (Choi et al. 2023; Choi et al. 2022; Schneider et al. 2022; Schneider et al. 2023). All figures were generated using Python (version 3.9.13), R (version 4.4.0), and FreeSurfer (version 7.4.1).

DATA PROCESSING FOR BOLD-fMRI

BOLD signal processing

We analyzed a subsample of 53 participants—27 patients (11 female) and 26 healthy controls (15 females)—based on sufficient MRI for analysis (e.g., absence of motion artifacts and valid values in AICHA ROIs). Details on preprocessing and parcellation for rs-fMRI, including temporal band-pass filtering (0.01-0.1 Hz), spatial realignment, slice-time correction, motion correction, and registration to anatomical images, were described in previous works (Schneider et al. 2022; Schneider et al. 2023).

For each individual subject, EPI fMRI data were parcellated using the Atlas of Intrinsic Connectivity of Homotopic Areas (AICHA) (Joliot et al. 2015) (**Fig. 2B**), which resulted in 192 pairs of homotopic ROIs, yielding a total of 384 cortical and subcortical gray matter ROIs (**Fig. 2C**).

BOLD time series were extracted from the 192 homotopic ROI pairs, and Z-score normalization was applied prior to power spectral density (PSD), coherence, and correlation analyses. Z-score normalization was computed as $z = (x - \mu)/\sigma$, where x represents the original fMRI time series and μ and σ denote its mean and the standard deviation, respectively (using the 'zscore' function in MATLAB). In representative cases—a healthy control and a patient with unilateral ICAS (**Fig. 2E, F, J,** and **K**)—Z-score normalized fMRI time series were averaged across homotopic ROI pairs to illustrate differences in temporal patterns (**Fig. 2D** and **E**). To more specifically compare infra-slow oscillations (<0.1 Hz), representative Z-score

normalized fMRI time series were also extracted from one homotopic ROI pair (precuneus) and one heterotopic ROI pair (precuneus and lingual gyrus) in both subjects (**Fig. 2J,** and **K**).

PSD analysis

Z-score normalized fMRI time series were transformed into PSD values to assess amplitude differences in resting-state BOLD signal power between the two groups. In the representative subjects, bilateral rs-fMRI signals were compared in the typical resting-state frequency band, 0.01-0.1 Hz (Fox and Raichle 2007; Cordes et al. 2001; He et al. 2018; Choi et al. 2022; Choi et al. 2023; Schneider et al. 2022; Schneider et al. 2023) (**Fig. 2F**). To quantify inter-hemispheric differences, PSD differences between the left and right hemispheres were summed across all homotopic ROI pairs and converted to absolute values, $|\Sigma(\Delta_{LR}\ PSD)| = |\Sigma(PSD_{Left} - PSD_{Right}|$, at two distinct frequency bands; 0.01-0.05 Hz and 0.08-0.1 Hz (**Fig. 2G**). PSD estimation was performed using Welch's method ('pwelch' function in MATLAB) with a Hamming window length of 128, Fast Fourier transform (FFT) length of 100, and 50% overlap. The frequency resolution was 1/120 s = 0.0083 Hz. The two distinct frequency bands were 0.01-0.05 Hz (referred to as <0.05 Hz) and 0.08-0.1 Hz (referred to as ~0.1 Hz in the following).

Spectral coherence analysis

Coherence analysis was employed to investigate the spectral dynamics of inter-hemispheric FC, as coherence is widely regarded as a frequency-domain measure of FC (He et al. 2018; Choi et al. 2022; Choi et al. 2023; Sun, Miller, and D'Esposito 2004; Yaesoubi et al. 2015). Higher coherence coefficients are generally interpreted as indicating stronger FC, whereas lower coefficients suggest reduced FC. In this study, spectral coherence was treated as a key marker for frequency-specific inter-hemispheric FC. To examine differences in coherence patterns between healthy controls and patients with unilateral ICAS, group-averaged spectral coherence was analyzed for both homotopic and heterotopic FC across the infra-slow frequency range (<0.1 Hz), specifically focusing on two distinct frequency bands: <0.05 Hz and ~0.1 Hz. Z-score normalized fMRI time series were used for coherence calculations to eliminate potential bias stemming from the baseline signal intensity differences between two hemispheres.

The coherence coefficient between two signals x and y—representing either homotopic or heterotopic ROI pairs—is defined as follows:

$$Coherence_{xy}(f) = \frac{\left|P_{xy}(f)\right|^2}{P_{xx}(f) * P_{yy}(f)}$$

where $P_{xx}(f)$ and $P_{yy}(f)$ denote the auto spectral densities of signals x and y, respectively, and $P_{xy}(f)$ is the cross-spectral density between them.

Coherence was computed using the magnitude-squared coherence estimate method ('mscohere' function in MATLAB, Mathworks, Natick, MA) with a hamming window length: 128, FFT length: 100, overlap: 50%). As in the PSD analysis, the frequency resolution was 1/120 s = 0.0083 Hz, allowing for the characterization of coherence patterns across the infra-slow oscillatory frequency range (<0.1 Hz). Two distinct frequency bands were examined: 0.01-0.05 Hz (referred to as <0.05 Hz) and 0.08-0.1 Hz (referred as to ~0.1 Hz). To facilitate group-level comparison, coherence coefficients between inter-hemispheric ROIs were Fisher Z-transformed prior to averaging within each frequency bands and group (Corey, Dunlap, and Burke 1998) (**Fig. 2L-N**).

Temporal correlation analysis

To complement the coherence analysis, temporal correlation analysis was conducted to assess inter-hemispheric FC across homotopic and heterotopic ROI pairs. As in the coherence analysis, Z-score normalized fMRI time series were used for both healthy controls and patients with unilateral ICAS.
The Pearson correlation coefficient between two signals x and y is defined as the following equation:

$$Correlation_{xy}(a,b) = \frac{\sum_{i=1}^{n}(x_{a,i} - \bar{x}_a)(y_{b,i} - \bar{y}_b)}{\sqrt{\sum_{i=1}^{n}(x_{a,i} - \bar{x}_a)^2 \sum_{i=1}^{n}(y_{b,i} - \bar{y}_b)^2}}$$

where x and y are the fMRI time series from ROIs a and b, respectively; i indicates the time points; and $\bar{x}_a$, $\bar{y}_b$ are the mean values of each time series.

Correlation coefficients were computed using 'corr' function in MATLAB (type: Pearson, rows: pairwise). As with coherence, Fisher-Z transform was applied to correlation values prior to averaging across inter-hemispheric ROI pairs within each group (**Fig. S5 A**).

Network-specific FC analysis

To assess the regional specificity of inter-hemispheric rs-fMRI, seven canonical rs-fMRI networks were utilized as defined by Yeo and colleagues (Yeo et al. 2011). These networks were derived from a dataset of 1,000 healthy individuals scanned on 3T Tim Trio MRI scanners (Siemens, Erlangen, Germany), and are widely used to characterize large-scale distributed network organization in human fMRI research. The seven networks included: Default Mode Network (DMN), Somatomotor Network (SMN), Dorsal Attention Network (DAN), Visual Network (VIN), Salience Network (SAN), Limbic Network (LIN), and Executive Control Network (ECN). In addition, subcortical network (SubCort) was delineated.

For network-specific FC analysis, inter-hemispheric coherence matrices were computed using homotopic and heterotopic AICHA ROI pairs across the infra-slow frequency band (0.01-0.1 Hz). Each AICHA ROI was assigned to one of the canonical rs-fMRI networks based on spatial overlap with the AICHA atlas (Joliot et al. 2015) and Yeo's network parcellation (Yeo et al. 2011), following procedures described by Labache et al. (Labache et al. 2023) (**Fig. 3A**). The coherence matrices were then reordered for each participant group (healthy controls and patients with unilateral ICAS) according to the canonical networks order: VIN, SMN, DAN, SAN, LIN, ECN, DMN, and SubCort. The reordered coherence matrices were averaged across three infra-slow frequency bands: the full infra-slow band (0.01-0.1 Hz; **Fig. 3B**), a lower-frequency band (0.01-0.05 Hz; **Fig. 3C**), and a higher-frequency band (0.08-0.1 Hz; **Fig. 3E**). Fisher-Z transform was applied prior to averaging and inverted after averaging to ensure appropriate statistical treatments. To assess regional specificity of inter-hemispheric FC across the networks, coherence values were averaged within each network for the two distinct frequency bands (<0.05 Hz and ~0.1 Hz) (**Fig. 3D** and 3**F**). Detailed information on the mapping of AICHA ROIs to canonical networks is provided in the Supplementary **Table S1**).

Identification of distinct perfusion territory

In patients with ICAS, the most vulnerable brain regions are located in the watershed areas, as these regions are particularly susceptible to reductions in CBF. Watershed areas are located at the cortical border zones between major arterial territories—namely, of the anterior, middle, and posterior cerebral arteries (ACA, MCA, and PCA)—as well as at internal border zone between lateral lenticulo-striate arteries (LSA) and

MCA (Torvik 1984; Momjian-Mayor and Baron 2005; Kaczmarz et al. 2021) (**Fig. 4A**). Because these regions are furthest from primary arterial supply and depend on distal branches of the major arteries, watershed areas can be defined based on temporal perfusion delay (Kaczmarz et al. 2018).

In this study, individual watershed areas were identified using DSC MRI-derived time-to-peak (TTP) maps, following the method described by Kaczmarz and colleagues (Kaczmarz et al. 2018; Kaczmarz et al. 2021). To alleviate variability in the definition and boundaries of watershed areas and to ensure spatial alignment with AICHA ROIs, a group-level watershed area mask was generated by averaging the individual masks across subjects (n = 52; one patient was excluded due to insufficient data quality) Based on the spatial overlap between the AICHA atlas and the group-defined watershed regions, AICHA ROIs were assigned to the watershed territory using a threshold of 95% overlap. A total of 41 ROI pairs, spanning canonical rs-fMRI networks and subcortical regions, were identified and confirmed though additional visual inspection. The watershed area mask was computed using visualization tools from Nilearn Python library (https://nilearn.github.io/dev/modules/plotting.html) and array transformation functions from Numpy Python library (https://numpy.org).

Spectral PSD and coherence analyses inside and outside watershed Areas.

To compare different spectral dynamics of PSDs and coherence inside versus outside the watershed areas, the absolute values of interhemispheric PSD differences were summed across homotopic ROI pairs located either inside or outside watershed areas. These summed differences, $|\Sigma(\Delta_{LR}\ \mathrm{PSD})|$, were computed separately for the two distinct frequency bands; 0.05 Hz and ~0.1 Hz. The resulting values were then compared between the two groups (**Fig. 4C**). Similarly, coherence values between homotopic or heterotopic ROI pairs were calculated separately for inside and outside the watershed area. Fisher Z-transform was applied prior to averaging, and inverse Fisher Z-transform was applied after averaging coherence values across ROI pairs, separately for the two distinct frequency bands in each group (**Fig. 4D**, **S2 A**, and **S3 A**).

For network-specific analyses of FC inside and outside watershed areas, AICHA ROIs overlapping with the defined watershed territory were reordered according to the canonical rs-fMRI networks and subcortical regions. Network-specific coherence matrices were then averaged across the two distinct frequency bands (<0.05 Hz and ~0.1 Hz), separately for regions inside and outside the watershed areas in each group. Fisher Z-transformation was applied prior to averaging coherence values across the networks, and inverse Z-transformation was performed after averaging. To visualize network-specific FC, circular diagrams were generated to represent the strength of coherence between the eight brain networks—comprising the seven canonical rs-fMRI networks and the subcortical network. Visualization was performed in R using 'ggraph' R library (package version 2.2.1). Detailed information on the AICHA ROIs overlapping with the distinct perfusion territories (i.e., inside vs. outside watershed areas) is provided in the Supplementary Information (**Table S2-3**).

DATA PROCESSING FOR MULTIPARAMETRIC QUANTITATIVE MRI

Estimation of CBV, CBF, $CMRO_2$ and BOLD time lag in Gray Matter

Hemodynamic MRI parameter maps, i.e., relative CBV (from the DSC MRI), and CBF (from pCASL MRI), and relative OEF ≈ R2′/ CBV were calculated as described previously (Kaczmarz et al. 2021) (**Fig. S4**). Subsequently, relative $CMRO_2$ maps were estimated using the following equation:

$$CMRO_2 = C_a \times Y_a \times OEF \times CBF$$

where C_a is the oxygen carrying capacity of arterial blood (μmol O_2 per 100 ml blood) and Y_a is the hemoglobin oxygen saturation level of arterial blood. Following the work reported by An and colleagues (An et al. 2001), we assumed that $Y_a \approx 1$ and $C_a = 0.19$ to simplify the estimation. To assess inter-hemispheric difference in BOLD time lag, lag time maps were generated from BOLD fMRI data using cross-correlation analysis in both groups. For each AICHA ROI, lag times were calculated as the time shift (ranging from -20 to +20 TRs) that maximized the cross-correlation coefficient with the fMRI signal from superior sagittal sinus. This analysis was implemented using the Python toolbox 'rapiditide', as described previously (Schneider et al. 2023). Detailed signal processing steps were provided in previous works (Schneider et al. 2022; Schneider et al. 2023).

Inter-hemispheric differences in multiparametric quantitative MRI

To assess individual MRI parameter maps (CBV, CBF, $CMRO_2$, and BOLD time lag), individual parameter maps were first parcellated using the AICHA atlas (Joliot et al. 2015). To compare differences between homotopic ROI pairs located inside versus outside the watershed areas, absolute inter-hemispheric differences were computed for each parameter. Specifically, for each subject, the absolute differences between left and right hemispheres were summed across homotopic ROI pairs using the following equation: $|\Sigma(\Delta_{LR}\ \text{MRI Parameter})| = |\Sigma(\text{MRI Parameter}_{\text{Left}} - \text{MRI Parameter}_{\text{Right}}|$. This calculation was performed separately for ROIs inside and outside the watershed areas (**Fig. 4I-J**).

STASTICAL ANALYSIS

To assess group differences in PSD and coherence, two-sample t-tests were performed to compare the mean values between healthy controls and patients with unilateral ICAS, considering p-values < 0.05 or < 0.01 statistically significant. For coherence analysis, Fisher-Z transform was applied to the coherence coefficient prior to the t-test to satisfy the model assumption (i.e., normal distribution). For comparison of inter-hemispheric differences in quantitative hemodynamic MRI parameters (CBV, CBF, $CMRO_2$, and BOLD time lag), Wilcoxon rank-sum tests were used to evaluate differences between the two groups separately for inside and outside of watershed, using the same significant thresholds (p-values < 0.05 or < 0.01).

Data availability

Availability of human subject data is restricted due to data privacy regulations. Data sharing requires specific ethics votes and data transfer agreements. Processed non-image data generated during this study are available from the corresponding author upon reasonable request.

Code availability

The related image processing codes are available from the corresponding author upon reasonable request.

Acknowledgements

We thank Jacob Duckworth, Drs. David Kleinfeld, Filip Sobczak, Loïc Labache, and Afra Wohlschläger for their helpful comments and discussions. We also thank Yehwan (Issac) Choi for his schematic illustrations. This work was supported the Deutsche Forschungsgemeinschaft (DFG, German Research

Foundation) – project number 395030489 and ev. Studienwerk Villigst (personal grant to Gabriel Hoffmann).

Author contributions

C.P. and C.S. designed and supervised the research, S.K. and C.P. performed experiments and acquired data, S.C. analyzed data, G.H., and S.S. provided technical support, S.C., X.Y., C.S., and C.P. wrote the manuscript.

Competing interests

S.K. is an employee of Philips GmbH Market DACH, Hamburg, Germany. X.Y. is a co-founder of MRIBOT LLC. The remaining authors declare no conflict of interest.

Additional information

Supplementary material for this paper can be found at the journal website.

REFERENCES

Aalkjær, C., D. Boedtkjer, and V. Matchkov. 2011. 'Vasomotion - what is currently thought?', *Acta Physiologica*, 202: 253-69.

Alsop, D. C., J. A. Detre, X. Golay, M. Gunther, J. Hendrikse, L. Hernandez-Garcia, H. Lu, B. J. MacIntosh, L. M. Parkes, M. Smits, M. J. van Osch, D. J. Wang, E. C. Wong, and G. Zaharchuk. 2015. 'Recommended implementation of arterial spin-labeled perfusion MRI for clinical applications: A consensus of the ISMRM perfusion study group and the European consortium for ASL in dementia', *Magn Reson Med*, 73: 102-16.

An, H., W. Lin, A. Celik, and Y. Z. Lee. 2001. 'Quantitative measurements of cerebral metabolic rate of oxygen utilization using MRI: a volunteer study', *NMR Biomed*, 14: 441-7.

Avirame, K., A. Lesemann, J. List, A. V. Witte, S. J. Schreiber, and A. Floel. 2015. 'Cerebral autoregulation and brain networks in occlusive processes of the internal carotid artery', *J Cereb Blood Flow Metab*, 35: 240-7.

Bilecen, D., E. W. Radu, A. C. Schulte, J. Hennig, K. Scheffler, and E. Seifritz. 2002. 'fMRI of the auditory cortex in patients with unilateral carotid artery steno-occlusive disease', *J Magn Reson Imaging*, 15: 621-7.

Biondetti, E., J. Cho, and H. Lee. 2023. 'Cerebral oxygen metabolism from MRI susceptibility', *Neuroimage*, 276: 120189.

Birn, R. M. 2012. 'The role of physiological noise in resting-state functional connectivity', *Neuroimage*, 62: 864-70.

Boittin, F. X., N. Macrez, G. Halet, and J. Mironneau. 1999. 'Boittin FX, Macrez N, Halet G, Mironneau J. Norepinephrine-induced Ca(2+) waves depend on InsP(3) and ryanodine receptor activation in vascular myocytes.', *American Physiological Society*, 277: 139-51.

Broggini, T., J. Duckworth, X. Ji, R. Liu, X. Xia, P. Machler, I. Shaked, L. P. Munting, S. Iyengar, M. Kotlikoff, S. J. van Veluw, M. Vergassola, G. Mishne, and D. Kleinfeld. 2024. 'Long-wavelength traveling waves of vasomotion modulate the perfusion of cortex', *Neuron*, 112: 2349-67 e8.

Caballero-Gaudes, C., and R. C. Reynolds. 2017. 'Methods for cleaning the BOLD fMRI signal', *Neuroimage*, 154: 128-49.

Chang, C., J. P. Cunningham, and G. H. Glover. 2009. 'Influence of heart rate on the BOLD signal: the cardiac response function', *Neuroimage*, 44: 857-69.

Cheng, H. L., C. J. Lin, B. W. Soong, P. N. Wang, F. C. Chang, Y. T. Wu, K. H. Chou, C. P. Lin, P. C. Tu, and I. H. Lee. 2012. 'Impairments in cognitive function and brain connectivity in severe asymptomatic carotid stenosis', *Stroke*, 43: 2567-73.

Choi, S., Y. Chen, H. Zeng, B. Biswal, and X. Yu. 2023. 'Identifying the distinct spectral dynamics of laminar-specific interhemispheric connectivity with bilateral line-scanning fMRI', *J Cereb Blood Flow Metab*, 43: 1115-29.

Choi, S., H. Zeng, Y. Chen, F. Sobczak, C. Qian, and X. Yu. 2022. 'Laminar-specific functional connectivity mapping with multi-slice line-scanning fMRI', *Cereb Cortex*, 32: 4492-501.

Cordes, D., V. M. Haughton, K. Arfanakis, J. D. Carew, P. A. Turski, C. H. Moritz, M. A. Quigley, and M. E. Meyerand. 2001. 'Frequencies contributing to functional connectivity in the cerebral cortex in "resting-state" data', *AJNR Am J Neuroradiol*, 22: 1326-33.

Corey, D. M., W. P. Dunlap, and M. Burke. 1998. 'Averaging Correlations: Expected Values and Bias in Combined Pearson rs and Fisher's z Transformations', *The Journal of General Psychology*, 125: 245-61.

Di Marco, L. Y., E. Farkas, C. Martin, A. Venneri, and A. F. Frangi. 2015. 'Is Vasomotion in Cerebral Arteries Impaired in Alzheimer's Disease?', *J Alzheimers Dis*, 46: 35-53.

Drew, P. J., C. Mateo, K. L. Turner, X. Yu, and D. Kleinfeld. 2020. 'Ultra-slow Oscillations in fMRI and Resting-State Connectivity: Neuronal and Vascular Contributions and Technical Confounds', *Neuron*, 107: 782-804.

Fox, M. D., and M. E. Raichle. 2007. 'Spontaneous fluctuations in brain activity observed with functional magnetic resonance imaging', *Nat Rev Neurosci*, 8: 700-11.

Gleissner, C., S. Kaczmarz, J. Kufer, L. Schmitzer, M. Kallmayer, C. Zimmer, B. Wiestler, C. Preibisch, and J. Gottler. 2022. 'Hemodynamic MRI parameters to predict asymptomatic unilateral carotid artery stenosis with random forest machine learning', *Front Neuroimaging*, 1: 1056503.

Gotoh, F. , Y. Fukuuchi, H. Okayasu, K. Tanaka, N. Suzuki, and M. Kobari. 1982. 'Rhythmic changes in diameter of pial vessels and function of autonomic nervous system.', *Cerebral Blood Flow: Effects of Nerves and Neuro-transmitters, edited by Heistad DD. Amsterdam: Elsevier North Holland*: 409-17.

Gottler, J., S. Kaczmarz, M. Kallmayer, I. Wustrow, H. H. Eckstein, C. Zimmer, C. Sorg, C. Preibisch, and F. Hyder. 2019. 'Flow-metabolism uncoupling in patients with asymptomatic unilateral carotid artery stenosis assessed by multi-modal magnetic resonance imaging', *J Cereb Blood Flow Metab*, 39: 2132-43.

Gottler, J., S. Kaczmarz, R. Nuttall, V. Griese, N. Napiorkowski, M. Kallmayer, I. Wustrow, H. H. Eckstein, C. Zimmer, C. Preibisch, K. Finke, and C. Sorg. 2020. 'The stronger one-sided relative hypoperfusion, the more pronounced ipsilateral spatial attentional bias in patients with asymptomatic carotid stenosis', *J Cereb Blood Flow Metab*, 40: 314-27.

Gur, A. Y., and N. M. Bornstein. 2006. 'Cerebral vasomotor reactivity of bilateral severe carotid stenosis: is stroke unavoidable?', *Eur J Neurol*, 13: 183-6.

Gur, AY. , I. Bova, and NM. Bornstein. 1996. 'Is impaired cerebral vasomotor reactivity a predictive factor of stroke in asymptomatic patients?', *Stroke*, 27(12): 2188-90.

He, Y., M. Wang, X. Chen, R. Pohmann, J. R. Polimeni, K. Scheffler, B. R. Rosen, D. Kleinfeld, and X. Yu. 2018. 'Ultra-Slow Single-Vessel BOLD and CBV-Based fMRI Spatiotemporal Dynamics and Their Correlation with Neuronal Intracellular Calcium Signals', *Neuron*, 97: 925-39 e5.

Holstein-Ronsbo, S., Y. Gan, M. J. Giannetto, M. K. Rasmussen, B. Sigurdsson, F. R. M. Beinlich, L. Rose, V. Untiet, L. M. Hablitz, D. H. Kelley, and M. Nedergaard. 2023. 'Glymphatic influx and clearance are accelerated by neurovascular coupling', *Nat Neurosci*, 26: 1042-53.

Hudetz, A. G., R. J. Roman, and D. R. Harder. 1992. 'Spontaneous flow oscillations in the cerebral cortex during acute changes in mean arterial pressure', *J Cereb Blood Flow Metab*, 12: 491-9.

Hundley, W. G., G. J. Renaldo, J. E. Levasseur, and H. A. Kontos. 1988. 'Vasomotion in cerebral microcirculation of awake rabbits', *Am J Physiol*, 254: H67-71.

Intaglietta, M. 1990. 'Vasomotion and flowmotion: physiological mechanisms and clinical evidence', *Vascular Medicine Review*, 1(2): 101-12.

Ishikawa, H., A. Shindo, A. Mizutani, H. Tomimoto, E. H. Lo, and K. Arai. 2023. 'A brief overview of a mouse model of cerebral hypoperfusion by bilateral carotid artery stenosis', *J Cereb Blood Flow Metab*, 43: 18-36.

Joliot, M., G. Jobard, M. Naveau, N. Delcroix, L. Petit, L. Zago, F. Crivello, E. Mellet, B. Mazoyer, and N. Tzourio-Mazoyer. 2015. 'AICHA: An atlas of intrinsic connectivity of homotopic areas', *J Neurosci Methods*, 254: 46-59.

Jones, T. W. 1852. 'Discovery that the veins of the bat's wing are endowed with rhythmical contractility and that onward flow of blood is accelerated by each contraction.', *Philosophical Transactions of the Royal Society of London*, 142: 131-36.

Julien, C. 2006. 'The enigma of Mayer waves: Facts and models', *Cardiovasc Res*, 70: 12-21.

Kaczmarz, S., J. Gottler, J. Petr, M. B. Hansen, K. Mouridsen, C. Zimmer, F. Hyder, and C. Preibisch. 2021. 'Hemodynamic impairments within individual watershed areas in asymptomatic carotid artery stenosis by multimodal MRI', *J Cereb Blood Flow Metab*, 41: 380-96.

Kaczmarz, S., V. Griese, C. Preibisch, M. Kallmayer, M. Helle, I. Wustrow, E. T. Petersen, H. H. Eckstein, C. Zimmer, C. Sorg, and J. Gottler. 2018. 'Increased variability of watershed areas in patients with high-grade carotid stenosis', *Neuroradiology*, 60: 311-23.

Kaczmarz, S., F. Hyder, and C. Preibisch. 2020. 'Oxygen extraction fraction mapping with multi-parametric quantitative BOLD MRI: Reduced transverse relaxation bias using 3D-GraSE imaging', *Neuroimage*, 220: 117095.

Kilic, K., and A. Devor. 2023. 'The stop and go of glymphatic flow', *Nat Neurosci*, 26: 924-25.

Kleinfeld, D., P. P. Mitra, F. Helmchen, and W. Denk. 1998. 'Fluctuations and stimulus-induced changes in blood flow observed in individual capillaries in layers 2 through 4 of rat neocortex', *Proc Natl Acad Sci U S A*, 95: 15741-6.

Labache, L., T. Ge, B. T. T. Yeo, and A. J. Holmes. 2023. 'Language network lateralization is reflected throughout the macroscale functional organization of cortex', *Nat Commun*, 14: 3405.

Margulies, D. S., S. S. Ghosh, A. Goulas, M. Falkiewicz, J. M. Huntenburg, G. Langs, G. Bezgin, S. B. Eickhoff, F. X. Castellanos, M. Petrides, E. Jefferies, and J. Smallwood. 2016. 'Situating the default-mode network along a principal gradient of macroscale cortical organization', *Proc Natl Acad Sci U S A*, 113: 12574-79.

Mateo, C., P. M. Knutsen, P. S. Tsai, A. Y. Shih, and D. Kleinfeld. 2017. 'Entrainment of Arteriole Vasomotor Fluctuations by Neural Activity Is a Basis of Blood-Oxygenation-Level-Dependent "Resting-State" Connectivity', *Neuron*, 96: 936-48 e3.

Mayhew, J. E., S. Askew, Y. Zheng, J. Porrill, G. W. Westby, P. Redgrave, D. M. Rector, and R. M. Harper. 1996. 'Cerebral vasomotion: a 0.1-Hz oscillation in reflected light imaging of neural activity', *Neuroimage*, 4: 183-93.

Mitra, P. P., S. Ogawa, X. Hu, and K. Ugurbil. 1997. 'The nature of spatiotemporal changes in cerebral hemodynamics as manifested in functional magnetic resonance imaging', *Magn Reson Med*, 37: 511-8.

Momjian-Mayor, I., and J. C. Baron. 2005. 'The pathophysiology of watershed infarction in internal carotid artery disease: review of cerebral perfusion studies', *Stroke*, 36: 567-77.

NASCET, SC. 1991. 'North American Symptomatic Carotid Endarterectomy Trial. Methods, patient characteristics, and progress', *Stroke*, 22: 711-20.

Nicoll, P. A., and R. L. Webb. 1955. 'Vascular patterns and active vasomotion as determiners of flow through minute vessels', *Angiology*, 6: 291-308.

Obrig, H., M. Neufang, R. Wenzel, M. Kohl, J. Steinbrink, K. Einhaupl, and A. Villringer. 2000a. 'Spontaneous low frequency oscillations of cerebral hemodynamics and metabolism in human adults', *Neuroimage*, 12: 623-39.

———. 2000b. 'Spontaneous low frequency oscillations of cerebral hemodynamics and metabolism in human adults', *Neuroimage*, 12: 623-39.

Raut, R. V., A. Z. Snyder, A. Mitra, D. Yellin, N. Fujii, R. Malach, and M. E. Raichle. 2021. 'Global waves synchronize the brain's functional systems with fluctuating arousal', *Sci Adv*, 7.

Rayshubskiy, A., T. J. Wojtasiewicz, C. B. Mikell, M. B. Bouchard, D. Timerman, B. E. Youngerman, R. A. McGovern, M. L. Otten, P. Canoll, G. M. McKhann, 2nd, and E. M. Hillman. 2014. 'Direct, intraoperative observation of ~0.1 Hz hemodynamic oscillations in awake human cortex: implications for fMRI', *Neuroimage*, 87: 323-31.

Razavi, M., B. Eaton, S. Paradiso, M. Mina, A. G. Hudetz, and L. Bolinger. 2008. 'Source of low-frequency fluctuations in functional MRI signal', *J Magn Reson Imaging*, 27: 891-7.

Reimer, J., M. J. McGinley, Y. Liu, C. Rodenkirch, Q. Wang, D. A. McCormick, and A. S. Tolias. 2016. 'Pupil fluctuations track rapid changes in adrenergic and cholinergic activity in cortex', *Nat Commun*, 7: 13289.

Reinhard, M., T. Muller, M. Roth, B. Guschlbauer, J. Timmer, and A. Hetzel. 2003. 'Bilateral severe carotid artery stenosis or occlusion - cerebral autoregulation dynamics and collateral flow patterns', *Acta Neurochir (Wien)*, 145: 1053-9; discussion 59-60.

Rodgers, Z. B., J. A. Detre, and F. W. Wehrli. 2016. 'MRI-based methods for quantification of the cerebral metabolic rate of oxygen', *J Cereb Blood Flow Metab*, 36: 1165-85.

Rosenblum, B. R., R. F. Bonner, and E. H. Oldfield. 1987. 'Intraoperative measurement of cortical blood flow adjacent to cerebral AVM using laser Doppler velocimetry', *J Neurosurg*, 66: 396-9.

Schneider, S. C., M. E. Archila-Melendez, J. Gottler, S. Kaczmarz, B. Zott, J. Priller, M. Kallmayer, C. Zimmer, C. Sorg, and C. Preibisch. 2022. 'Resting-state BOLD functional connectivity depends on the heterogeneity of capillary transit times in the human brain A combined lesion and simulation study about the influence of blood flow response timing', *Neuroimage*, 255: 119208.

Schneider, SC. , ME. Archila-Meléndez, J. Göttler, S. Kaczmarz, B. Zott, J. Priller, M. Kallmayer, C. Zimmer, C. Sorg, and C. Preibisch. 2023. 'Stronger influence of systemic than local hemodynamic-vascular factors on resting-state BOLD functional connectivity', *Neuroimage*, 281.

Seifert, H., K. Jager, and A. Bollinger. 1988. 'Analysis of flow motion by the laser Doppler technique in patients with peripheral arterial occlusive disease', *Int J Microcirc Clin Exp*, 7: 223-36.

Silvestrini, M., E. Troisi, M. Matteis, L. M. Cupini, and C. Caltagirone. 1996. 'Transcranial Doppler assessment of cerebrovascular reactivity in symptomatic and asymptomatic severe carotid stenosis', *Stroke*, 27: 1970-3.

Silvestrini, M., F. Vernieri, P. Pasqualetti, M. Matteis, F. Passarelli, E. Troisi, and C. Caltagirone. 2000. 'Impaired cerebral vasoreactivity and risk of stroke in patients with asymptomatic carotid artery stenosis', *JAMA*, 283: 2122-7.

Sun, F. T., L. M. Miller, and M. D'Esposito. 2004. 'Measuring interregional functional connectivity using coherence and partial coherence analyses of fMRI data', *Neuroimage*, 21: 647-58.

Torvik, A. 1984. 'The pathogenesis of watershed infarcts in the brain', *Stroke*, 15: 221-3.

Wardlaw, J. M., C. Smith, and M. Dichgans. 2019. 'Small vessel disease: mechanisms and clinical implications', *Lancet Neurol*, 18: 684-96.

Wiedeman, M. P. 1957. 'Effect of venous flow on frequency of venous vasomotion in the bat wing', *Circ Res*, 5: 641-4.

Williams, K. A., M. Magnuson, W. Majeed, S. M. LaConte, S. J. Peltier, X. Hu, and S. D. Keilholz. 2010. 'Comparison of alpha-chloralose, medetomidine and isoflurane anesthesia for functional connectivity mapping in the rat', *Magn Reson Imaging*, 28: 995-1003.

Yaesoubi, M., E. A. Allen, R. L. Miller, and V. D. Calhoun. 2015. 'Dynamic coherence analysis of resting fMRI data to jointly capture state-based phase, frequency, and time-domain information', *Neuroimage*, 120: 133-42.

Yeo, B. T., F. M. Krienen, J. Sepulcre, M. R. Sabuncu, D. Lashkari, M. Hollinshead, J. L. Roffman, J. W. Smoller, L. Zollei, J. R. Polimeni, B. Fischl, H. Liu, and R. L. Buckner. 2011. 'The organization of the human cerebral cortex estimated by intrinsic functional connectivity', *J Neurophysiol*, 106: 1125-65.

Zarrinkoob, L., A. Wahlin, K. Ambarki, R. Birgander, A. Eklund, and J. Malm. 2019. 'Blood Flow Lateralization and Collateral Compensatory Mechanisms in Patients With Carotid Artery Stenosis', *Stroke*, 50: 1081-88.

Zhang, Y. Y., J. Z. Li, H. Q. Xie, Y. X. Jin, W. T. Wang, B. Zhao, and J. M. Jia. 2024. 'High-resolution vasomotion analysis reveals novel arteriole physiological features and progressive modulation of cerebral vascular networks by stroke', *J Cereb Blood Flow Metab*, 44: 1330-48.

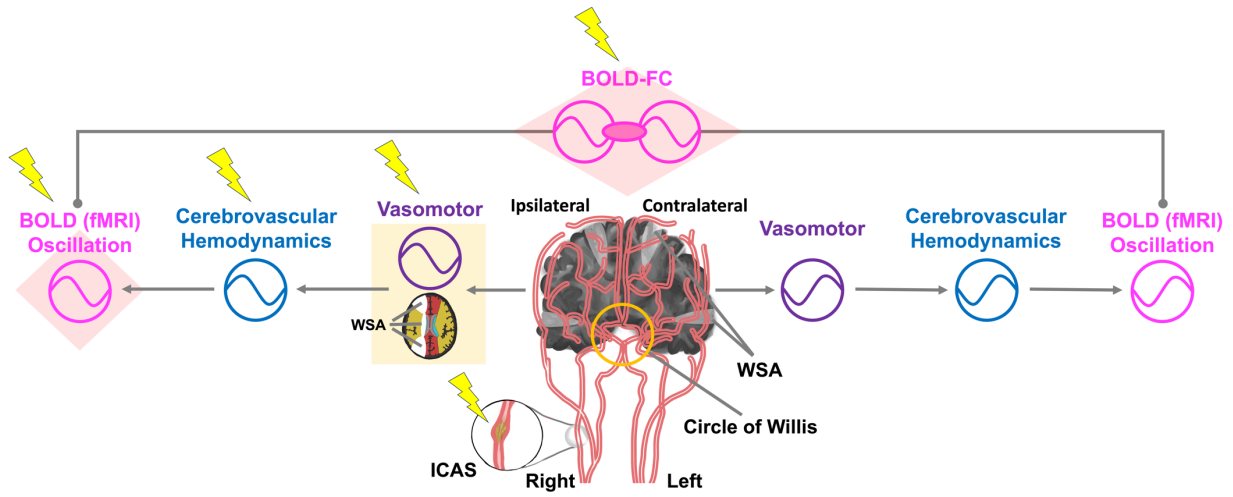

Figure 1. Conceptual cascade model of vasomotor-driven cerebrovascular hemodynamics and its impact on BOLD functional connectivity (FC). Unilateral internal carotid artery stenosis (ICAS, lightning symbol) leads to impaired vasomotor oscillations through shared vascular networks, particularly via the Circle of Willis. Disrupted vasomotion (right hemisphere ipsilateral to ICAS) alters downstream cerebrovascular hemodynamics, e.g., cerebral blood flow, cerebral blood volume, and cerebral metabolic rate of oxygen, particularly in vulnerable watershed areas (WSAs). These alterations result in disrupted frequency-specific BOLD oscillations and FC between two hemispheres, as measured by reduced inter-hemispheric coherence at the vasomotor frequency band (~0.1 Hz).

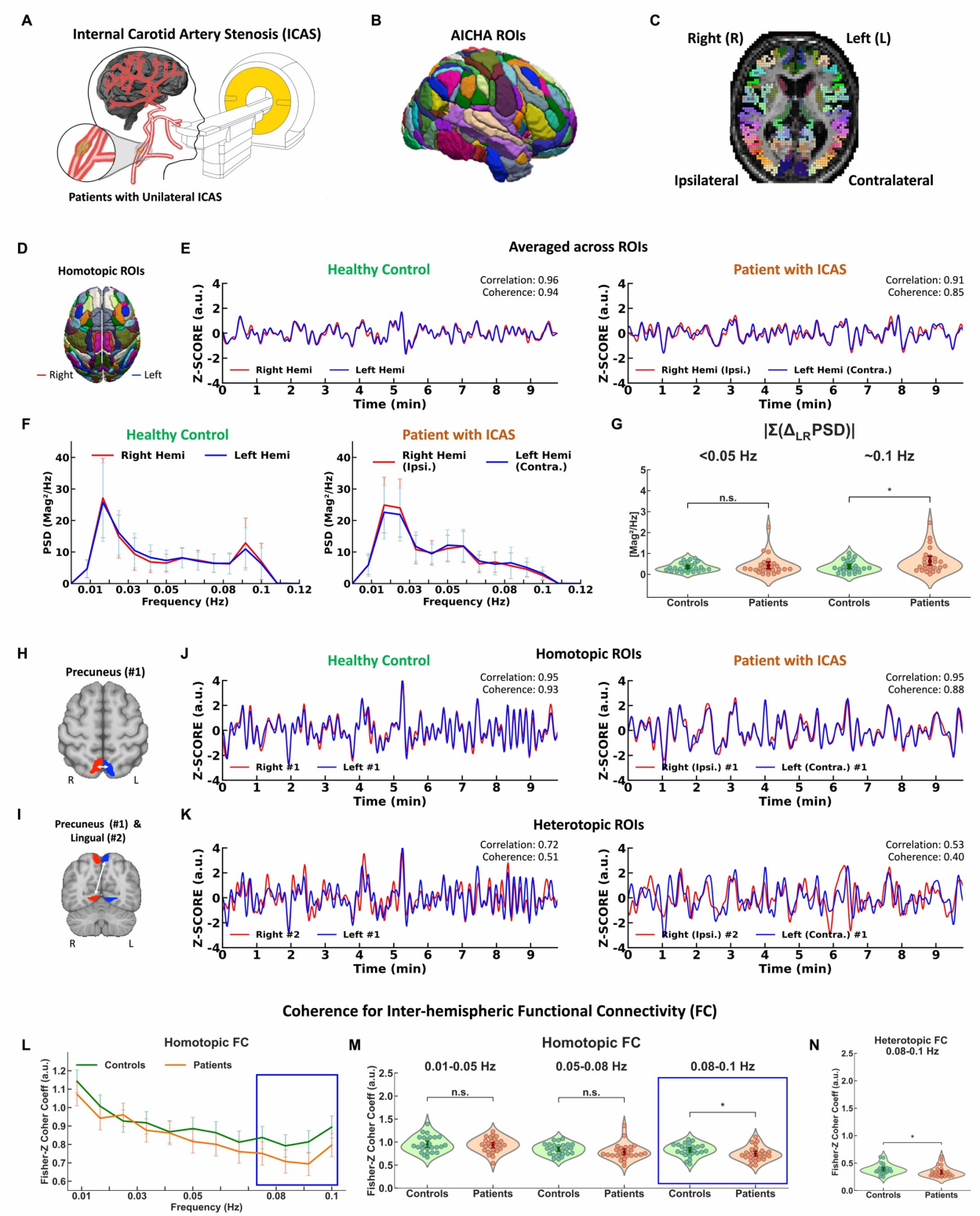

Figure 2. Frequency dependence of homotopic and heterotopic FC in healthy controls and patients with ICAS. A. Conceptual illustration of multi-modal MRI measurements in asymptomatic patients with

unilateral ICAS at 3T. **B.** Surface representation of AICHA brain parcellation (N = 384 ROIs). **C.** AICHA ROIs displayed on an axial T1-weighted MPRAGE image; identical colors indicate homotopic regions. **D. Illustration of homotopic ROI pairs defined by** AICHA atlas. **E.** Averaged Z-score normalized BOLD signal time series from right (red) and left (blue) hemispheres in a representative healthy control (left) and patient with ICAS (right). Correlation and coherence values are shown in each panel (top right). **F.** ROI-averaged PSD curves from the same representative healthy control (left) and patient with ICAS (right) shown in panel **E**. Error bars indicate mean ± SD across ROIs. **G.** Group-level absolute summed PSD differences between the left and right hemispheres, $|\Sigma(\Delta_{LR}\ \mathrm{PSD})|$ at <0.05 Hz and ~0.1 Hz (0.08-0.1 Hz) for healthy controls (green) and patients with ICAS (orange). **H** and **I.** AICHA ROIs corresponding to a representative homotopic ROI pair (**H**; Precuneus) and a heterotopic ROI pair (**I**; Precuneus and Lingual). Red and blue indicate right and left regions, respectively. **J** and **K.** Z-score normalized BOLD time series from the homotopic (**J**) and heterotopic (**K**) ROI pairs for the same representative subjects as in panel **E**. Correlation and coherence values are shown in each panel. **L** and **M.** Coherence for inter-hemispheric FC (healthy controls: green, patients with ICAS: orange). **L.** Group-level inter-hemispheric coherence (homotopic FC) at the infra-slow frequency band (0.01-0.1 Hz). The blue box marks the frequency range of ~0.08-0.1 Hz. Error bars indicate mean ± SEM across subjects. **M.** Comparison of homotopic FC across three distinct frequency bands: 0.01-0.05 Hz, 0.05-0.08 Hz, and 0.08-0.1 Hz (highlighted by blue box). **N.** Heterotopic FC at ~0.08-0.1 Hz. Statistical significance based on two-sample t-tests (∗: p-value < 0.05; n.s.: not significant). Diamond markers and outlines represent group means and 95% confidence intervals, respectively.

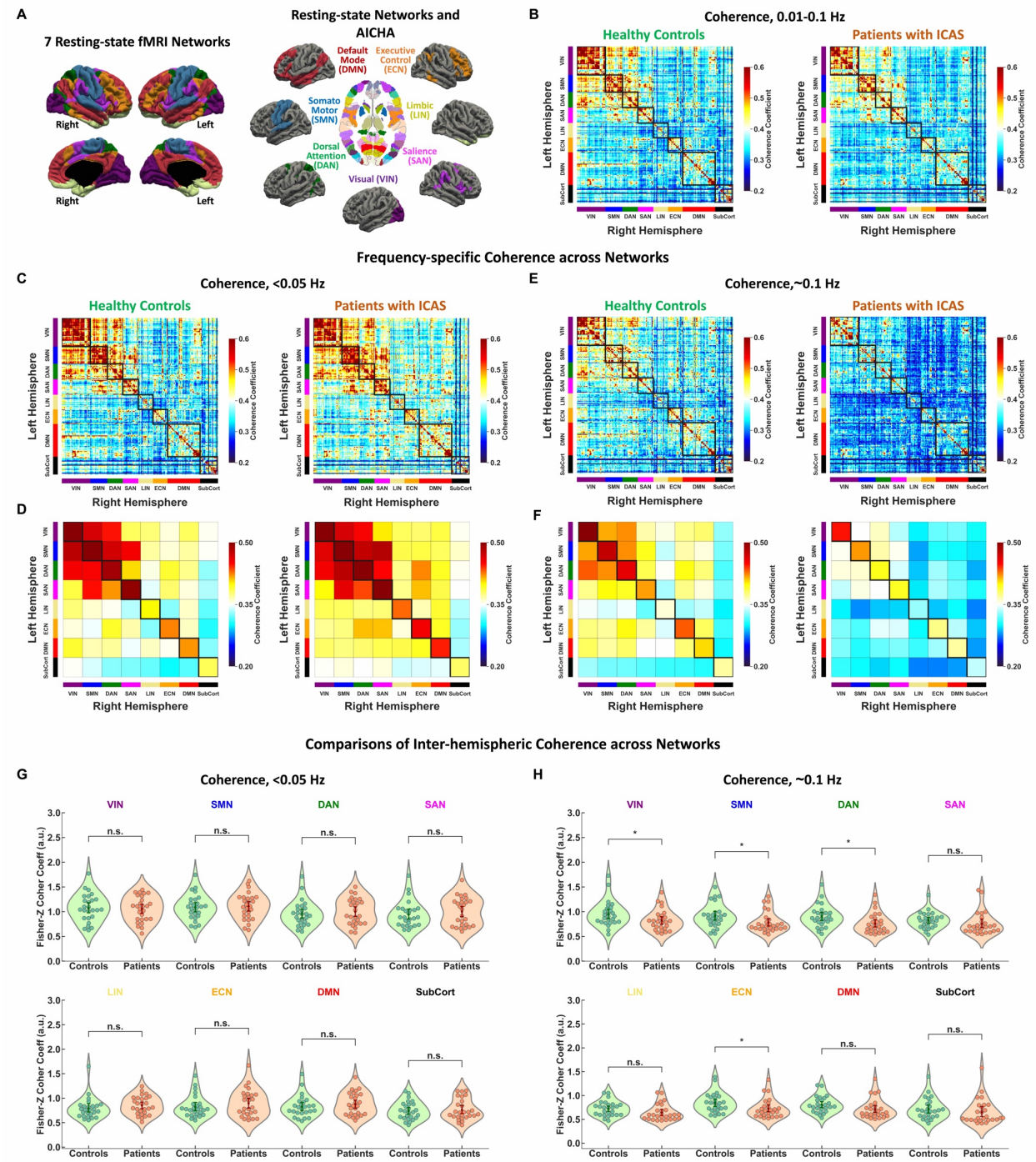

Figure 3. Frequency-dependent FC across networks in healthy controls and patients with ICAS. A. Surface representation of seven canonical rs-fMRI networks in right and left hemispheres (left), and their correspondence to AICHA ROIs (right). Overlapping AICHA ROIs were assigned to individual networks: Default Mode Network (DMN, red), Somatomotor Network (SMN, blue), Dorsal Attention Network (DAN, green), Visual Network (VIN, purple), Salience Network (SAN, magenta), Limbic Network (LIN, cream), and Executive Control Network (ECN, orange). The subcortical network (SubCort, black) was also included. **B-F.** Inter-hemispheric coherence matrices of reordered AICHA ROIs across networks for

healthy controls (left) and patients with ICAS (right). **B.** Coherence matrices for the full infra-slow frequency range (0.01-0.1 Hz). **C** and **D.** Frequency-specific coherence analysis at <0.05 Hz (0.01-0.05 Hz): **C.** Full network-level coherence matrices. **D.** Network-averaged coherence matrices across the eight networks. **E** and **F.** Frequency-specific coherence analysis at ~0.1 Hz (0.08-0.1 Hz): **E.** Full network-level coherence matrices. **F.** Network-averaged coherence. **G** and **H.** Group comparisons of inter-hemispheric coherence across networks between healthy controls (green) and patients with ICAS (orange): **G.** At <0.05 Hz. **H.** At ~0.1 Hz. Statistical comparisons were performed using two-sample *t*-tests (n.s.: no significance and ∗: p-value<0.05). Diamond markers and outlines represent group means and 95% confidence intervals.

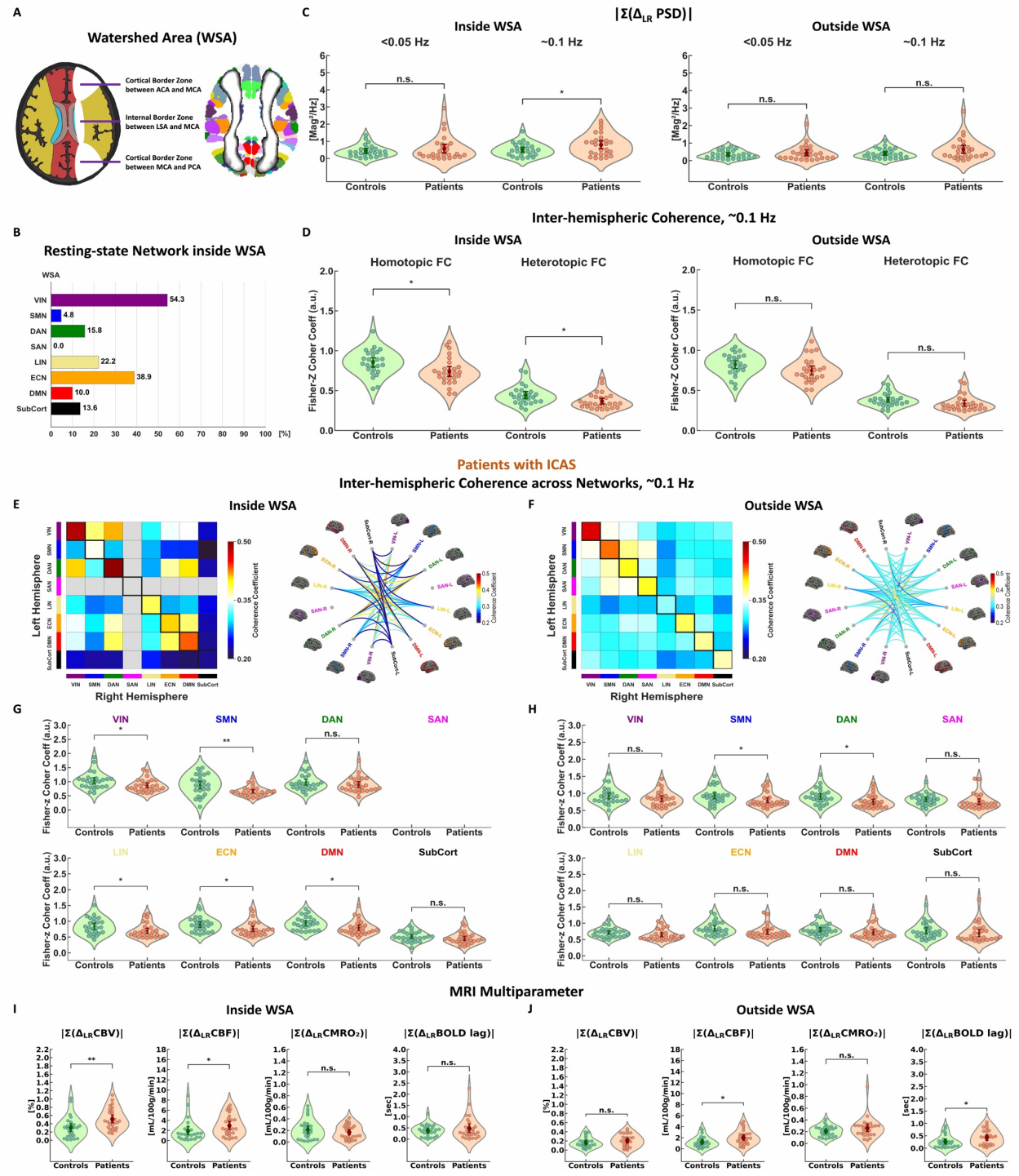

Figure 4. Frequency dependent FC inside and outside of watershed areas. A. Schematic illustration of **watershed areas** (WSAs, white), i.e., border zones: the cortical border zone between the anterior and middle cerebral arteries (ACA–MCA, top), the internal border zone between the lateral striate arteries (LSA) and MCA (middle), and the cortical border zone between the middle and posterior cerebral arteries (MCA–PCA, bottom). Right: Group-average bilateral WSA mask (white) from ICAS patients overlaid on the AICHA atlas (colored ROIs indicate homotopic regions). **B.** Proportional distribution of AICHA ROIs

within WSAs across resting-state networks and subcortical regions: VIN (visual network, purple): 54.3%, SMN (somatomotor network, blue): 4.8%, DAN (dorsal attention network, green): 15.8%, SAN (salience network): 0%, LIN (limbic network, cream): 22.2%, ECN (executive control network, orange): 38.9%, DMN (default mode network, red): 10.0%, and SubCort (subcortical regions, black): 13.6%. **C** and **D.** Group-level comparisons of inter-hemispheric PSD and coherence values inside and outside WSAs for healthy controls (green) and patients with ICAS (orange). **C.** Absolute inter-hemispheric PSD differences $|\Sigma(\Delta_{LR}\ \mathrm{PSD})|$ at <0.05 Hz and ~0.1 Hz (0.08-0.1 Hz). **D.** Inter-hemispheric coherence values for homotopic and heterotopic FCs inside (left) and outside WSAs (right). **E-H.** Network-specific inter-hemispheric coherence at ~0.1 Hz (0.08-0.1 Hz) in ICAS patients: **E** and **F.** Network-wise coherence matrix (left) and corresponding circular visualizations (right) inside (**E**) and outside (**F**) WSAs. Gray color in the SAN row and column (**E**) denotes unassigned values. **G** and **H.** Group comparisons of inter-hemispheric coherence across networks inside (**G**) and outside (**H**) WSAs. Two-sample t-tests were used to assess group differences (∗: p-value<0.05, n.s.: not significant). **I** and **J.** Group comparisons of inter-hemispheric differences in quantitative MRI parameters (CBV, CBF, $CMRO_2$, and BOLD time lag) inside (**I**) and outside (**J**) WSAs. Values represent absolute sums of left–right hemisphere differences ($|\Sigma(\Delta_{LR}\ \mathrm{MRI\ Parameter})|$). Wilcoxon rank-sum tests were used to assess statistical significance (∗: p-value < 0.05, ∗∗: p-value < 0.01, and n.s.: no significance). Diamond markers and outlines indicate group means and 95% confidence intervals.